Smectic-A–Smectic-C–Smectic-C^* Multicritical Point in Ferroelectric Liquid Crystals

Shankar B. Rananavare, V. G. K. M. Pisipati,* and E. W. Wong†
Oregon Graduate Institute, P.O. Box 91000, Portland, Oregon 97291-1000
(Received 9 February 1994)

We report a smectic-A–smectic-C–smectic-C^* (ACC^*) multicritical point in mixtures of chiral DOBAMBC [p-(n-decyloxy-benzylidene)-p-amino-(2-methyl-butyl)] cinnamate and achiral 10O.8 (4-decyloxybenzylidene-4-octylaniline). Studies of the phase diagram, tilt angle, polarization, and helix pitch indicate an ACC^* Lifshitz point describable by the extended Landau theory. Specifically, T_{AC^*} and the maximum polarization (P_m) exhibit quadratic composition dependence while the helical pitch length ($p = 2\pi/q$) varies linearly. Both q and P_m vanish discontinuously at the C-C^* boundary revealing its first order nature, consistent with a possible Lifshitz point.

PACS numbers: 64.70.Md, 61.20.–p

A Lifshitz point [1] represents an anomaly in a phase diagram along a second order phase transition line (λ line) where the coefficient of the gradient term(s) (Λ) vanishes. Emanating from the Lifshitz point (LP) is a line of first order transition that separates a modulated phase ($\Lambda > 0$) from an unmodulated phase ($\Lambda = 0$). The modulation wave vector (q) exhibits singular behavior as the LP is approached along the λ line [$q \sim (p - p_c)^{\beta_q}$, where p is a thermodynamic field variable such as composition, pressure, or electric (E) or magnetic (H) field]. Examples of LPs are known to occur in metamagnets [2] and microemulsions [3]. For liquid crystals [4], Chen and Lubensky [5] predicted that the nematic–smectic-A–smectic-C (NAC) multicritical point should be an LP as was later experimentally verified [6]. Michaelson [7] suggested, and later Blinc *et al.* [7] demonstrated a LP in field (H, cell thickness, and E) and temperature phase diagrams of the ferroelectric smectic-C^* (Sm-C^*) liquid crystalline (FLC) phase. In contrast, the present paper reports a novel smectic-A–smectic-C–smectic-C^* (ACC^*) multicritical point in *mixtures* of liquid crystals. Surprisingly, some aspects of phase topology are more readily accessible as a function of composition than field.

The ferroelectric smectic-C^* [4,8] phase (of C_2 rotational symmetry) is a layered phase that is density modulated in one dimension and is liquidlike in the other two (overall symmetry $G = Z \otimes C_2$). It is composed of orientationally aligned (along $\hat{\mathbf{n}}$, the director) chiral molecules which are tilted with respect to the layer normal (z). The azimuthal angle (ϕ) varies slightly from layer to layer tracing out a helix. In response to an electric field applied in the plane of the layers, the helix is unwound due to the alignment of the nonzero average layer dipole moment ($\equiv P$) perpendicular to the layer normal ($\hat{\mathbf{n}} \times \mathbf{z} = P \| C_2$ axis). Smectic-C (Sm-C) (tilted, C_{2h} symmetry) and smectic-A (Sm-A) (untilted, $D_{\infty h}$ symmetry) phases made up of achiral molecules are also one dimensionally modulated but lack the helical superstructure.

Field-induced ACC^* LPs in FLCs are complex and give rise to reentrant C^* phases and runaway Lifshitz points [7]. In view of this, we searched for the ACC^* point in simple binary mixtures, establishing a phase diagram of DOBAMBC/10O.8 mixtures using differential calorimetry and optical microscopy (Fig. 1). The primary reasons for selection of these liquid crystals are the following: (1) they both belong to the same homologous series (i.e., Schiff bases), (2) they have side chains of similar lengths, and (3) they exhibit C/C^* phases over roughly similar temperature extents. They should, therefore, form ideal solutions.

To measure macroscopic polarization (P) we have used liquid crystal cells [9] made up of unidirectionally rubbed, polyamide-coated ITO (indium titanium oxide) glass plates separated by thin (25 μm) Mylar spacers. The balanced capacitance bridge and triangular wave meth-

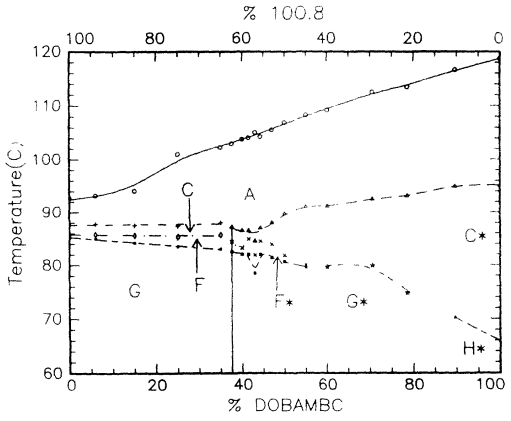

FIG. 1. Temperature composition phase digram of DOBAMBC and 10O.8 mixtures. The vertical line roughly (within 1%) divides the chiral phases (right) and achiral phases (left). Symbols I, A, $C(*)$, $F(*)$, $G(*)$, $H(*)$ refer to isotropic, smectic A, $C(*)$, $F(*)$, $G(*)$, and $H(*)$ phases. The uncertainity in AC^* transition temperatures is 0.2°C, and for the $C(*) - F(*)$ and $F(*) - G(*)$ transitions is 0.4°C. Smooth lines have been drawn through the transition data points to guide the eye.

0031-9007/94/72(22)/3558(4)$06.00

ods [10] were used to monitor P with better than 0.05 K temperature control. Optical microscopic measurements of fringe spacings and optical diffraction patterns in thick (> 100 μm) and homogeneously aligned samples were used to measure helix pitch lengths (p). Molecular tilt angles were determined from x-ray diffraction studies conducted on a temperature-controlled stage (± 0.1°C). Both molecules in their respective Sm-A phases exhibit similar layer thicknesses ($d_{11O.8,\mathrm{DOBAMBC}} = 33.35 \pm 0.04$ Å, 33.06 ± 0.04 Å) which decrease upon entering the C/C^* phases owing to the nonzero molecular tilt angle.

The AC/AC^* transition has been studied over the last two decades using a range of techniques, such as ac calorimetry and x-ray scattering [6,11]. The primary order parameter is molecular tilt with an easy rotation axis, i.e., it is described by a two-component, complex order parameter ($\Psi = \theta e^{i\phi} \equiv \xi_1 \hat{\mathbf{x}} + \xi_2 \hat{\mathbf{y}}$, de Genne's 3D XY model [4]). The extended Landau free energy for this transition is [12]

$$F(z) = \tfrac{1}{2}a(\xi_1^2+\xi_2^2) + \tfrac{1}{4}b(\xi_1^2+\xi_2^2)^2 + \tfrac{1}{6}c(\xi_1^2+\xi_2^2)^3 - [\Lambda + d(\xi_1^2+\xi_2^2)]\left(\xi_1\frac{d\xi_2}{dz} - \xi_2\frac{d\xi_1}{dz}\right) - \mu\left(P_x\frac{d\xi_2}{dz} + P_y\frac{d\xi_1}{dz}\right)$$
$$+\tfrac{1}{2}K_3\left[\left(\frac{d\xi_1}{dz}\right)^2 + \left(\frac{d\xi_2}{dz}\right)^2\right] + \frac{1}{2\epsilon}(P_x^2+P_y^2) + \frac{1}{4}\eta(P_x^2+P_y^2)^2 + C(P_x\xi_2 - P_y\xi_1) - \Omega(P_x\xi_2 - P_y\xi_1)^2. \quad (1)$$

The first three terms represent an order parameter expansion to the sixth order where $a = a_2(T_{AC^*} - T)/T^*$. b controls the order of the transition [first order ($b < 0$), second order ($b > 0$), or tricritical ($b = 0$)]. Most studies of second order AC/AC^* transitions [11] reveal anomalously large c coefficients forcing the expected 3D XY behavior very close to the transition $\Delta t \sim (1\text{–}5) \times 10^{-3}$. C_2 symmetry of the ferroelectric Sm-C^* phase allows three Lifshitz invariant terms associated with the spatial modulation of θ in the z direction (coefficients Λ and d) and a flexoelectric coupling term between P and θ (the μ term). P is a secondary order parameter with its magnitude being less than 1% of the molecular dipole moment. The $1/\epsilon$ and η coefficients define its expansion to the fourth order. Coefficients C and Ω are associated with piezoelectric and biquadratic coupling between θ and P. K_3 is an elastic constant. Carlsson *et al.* [12] have determined these values for DOBAMBC.

For the study of the AC^* and C-C^* transitions, we have conducted extensive measurements of q, P, and θ as functions of temperature and composition [13]. However, we focus here on data that are far from the AC^* transition line ($T_{C^*X} - T \approx 0.5$ K), since there is anomalous behavior of the pitch length in DOBAMBC attributed to the biquadratic coupling (Ω) term between P and θ. Figure 2 depicts the q variation as a function of the composition (x). Note that the pitch ($2\pi/q$) varies over an order of magnitude from 3.5 to 29 μms, disappearing discontinuously at the C-C^* transition occurring at 36% (i.e., $x_0 = 36$) of DOBAMBC. The pitch diverges (or q vanishes) with the power law exponent of -1 ($+1$) rather than $-1/2$ ($+1/2$) as predicted for the LP [1] because our measurements of the pitch length are not on the AC^* phase transition line.

A variation of q can be obtained by minimizing the free energy [Eq. (1)] with respect to q: $q = [\Lambda + \mu(P/\theta) + d\theta^2]/K_3$. Using the known values of these coefficients for DOBAMBC [12], measured $P_m(x)$ [Fig. 3(a)] and $\theta_m(x)$ [Fig. 3(b)] values, we find an increase in the pitch length, but only by a factor of 2. However, this neglects the concentration dependence of the coefficients in Eq. (1). In fact, the C_{2h} symmetry of the smectic-C phase forbids the Lifshitz variants. Hence, one may set Λ, d, and $\mu \sim x - x_0$, introducing a singular behavior for these constants leading to the observed linear variation of $q(x)$.

$P_m(x)$, shown in Fig. 3(a), decreases nonlinearly and disappears completely at $x_0 = 36$, further confirming the location of the C-C^* line shown in Fig. 1. $P_m(x)$ variation is neither linear (at fixed t, the reduced temperature) nor is it simply proportional to $\theta_m(x)$ [Fig. 3(b)]. $P_m(x)$ can be calculated by the extended mean field model using the singular behavior of the Lifshitz variants as discussed above. It yields $P(x)/\sin\theta(x) \approx A + B[(x - x_0)/(100 - x_0)]^2$ where $A = \epsilon C K_3/(K_3 - \mu^2\epsilon)$ and $B = \epsilon\mu(\Lambda + d\theta^2)/(K_3 - \mu^2\epsilon)$. This is consistent with the quadratic disappearance of $P_m(x)/\sin\theta_m(x)$ obtained by fitting the data in Fig. 3(a) (solid curve; $A = 2.11$, $B = 9.92$, and $\chi^2 = 2$).

The $\theta_m(x)$ variation (6°–21°), shown in Fig. 3(b), is remarkably similar to the $\theta(t)$ variation and it can

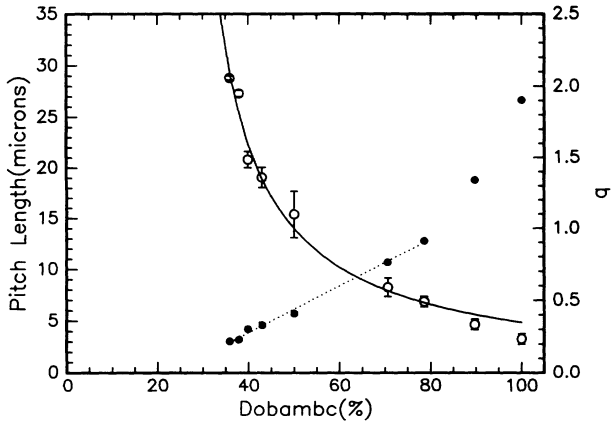

FIG. 2. Composition dependence of helical pitch (open symbols) or wave vector $q = 2\pi/p(\mu\mathrm{m})$ (closed symbols). Solid and dotted lines fit corresponding $q(p) = k_{q,p}(x - x')^{1(-1)}$ with $k_q = 375 \pm 36, x' = 23.2 \pm 1.5$, and $R = 0.97$, respectively.

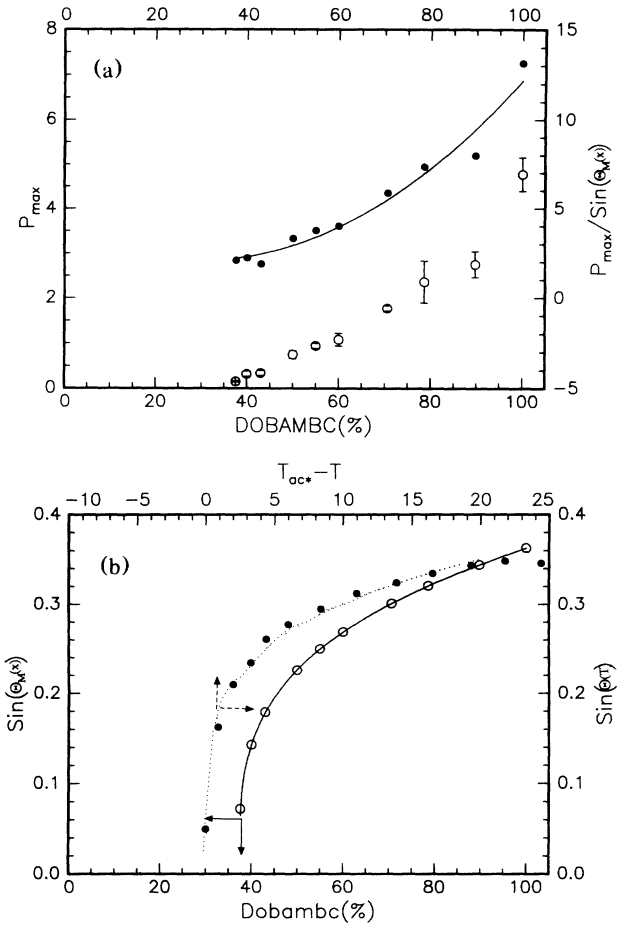

FIG. 3. (a) $P_m(x)$ vs composition (open circles). The top curve (closed circle) is $P_m(x)/\sin[\theta_m(x)]$ and the solid line is a fit by the quadratic form (see text). (b) $\sin\theta_{m(x)}$ vs composition (open circles). Solid line is a best fit by a power law yielding $\beta = 0.30 \pm 0.03$, and $\chi^2 = 1.6$. The top curve (closed circle) is $\sin[\theta(90,T)]$ with $\beta = 0.24 \pm 0.05$, $\chi^2 = 1.3$. Scales for these two data sets are marked with arrows.

be explained as follows: As the DOBAMBC concentration is reduced, $T_{C^*\text{-}X}$ ($X = H^*$, F^*, or F is the low temperature phase) increases linearly which in turn reduces t_m ($\propto T_{AC^*} - T_m$) almost linearly resulting in a power law decrease of $\theta \sim t^\beta$. This means, however, that for a fixed t, $\theta(x)$ varies slowly and linearly with x ($d\theta/dx = 0.082° \pm 0.0017°/\%$).

The phase diagram (Fig. 1) shows a quasilinear variation of T_{AC^*} that becomes quadratic with respect to x near the ACC^* point. Generally, such behavior is not seen in the field-dependent phase diagrams [12] where the estimate of the transition temperature dip is 0.2 K. In the extended Landau theory [Eq. (1)], the AC^* transition temperature shift is given by $\Delta T \approx (1/a_2)[\Lambda^2/K_3 +$ (higher order terms)]. In our phase diagram, which uses the composition variable to approach the LP, this temperature shift is about 2 K. This could be due to stronger reduction in a_2, which is known to dramatically decrease in materials exhibiting narrow Sm-A phase extent due to coupling of Sm-A and Sm-C order parameters [11]. Reduction in the Sm-A phase extent (for $x < 36$, Fig. 1) and the singular behavior for Λ accounts for the observed quadratic variation of T_{AC^*} near the ACC^* LP.

Interestingly, the phase diagram exhibits a transition from C to C^* phase at $x = 36$ and not at $x \sim 0$. This is remarkable since a 3%–4% concentration of chiral molecules typically converts a Sm-C phase to a chiral Sm-C^* phase. Moreover, the C-C^* transition line is almost vertical, which is similar to that found in field-dependent phase diagrams of the C-C^* transition. Such a result is accounted for by a soliton solution of a sine-Gordon equation obtained by adding appropriate electric, magnetic, or surface free energy terms to Eq. (1) [7,14]. The chemical potential term differs from these E, H, and surface field-dependent terms because it does not explicitly couple (linearly or quadratically) to P or θ. At present, a suitable model that incorporates an implicit coupling of the chemical potential and the order parameter, which would allow calculation of the C-C^* line, is not available.

In view of these difficulties, this discussion is restricted to qualitative aspects of the phase diagram developing simple analogies. A 3D XY axial next nearest neighbor model employing continuous spin variables, by Selke and Redner and Stanley [15] gives the location of the LP and a first order phase transition between modulated-unmodulated phases ($\equiv C^*$-C transition) in terms of the parameter, $\kappa \sim 1/4 \sim x$, which depends on the relative value of the three-spin vs two-spin coupling constants. The phase transition line rises vertically and meets the λ line, not at its minimum but at a slightly lower value of κ, consistent with our results at the ACC^* point (see Fig. 1). Notably, the molar value of x_0, separating chiral from achiral phases, is about 33% higher than the κ_{Lifshitz} value. It is likely that the actual value may even be closer to the estimate of 1/4, since we have not examined the curvature of the C-C^* transition line in the last 50 mK range before reaching the T_{ACC^*} point [16].

More insight into this behavior can be gained by drawing an analogy to a simple percolation model used in dilute magnetism [17]. The disappearance of the ferroelectric Sm-C^* phase coincides with the disappearance of the infinite cluster (i.e., $p > p_c$, where $p_c \equiv x_0$ is the percolation threshold). This leads to a vertical rise of the C-C^* phase boundary similar to a ferroparamagnetic (FP) phase transition. The numerical magnitude of the percolation threshold, which depends on the coordination number of the lattice, is similar to the 3D simple cubic lattice implying weak three-spin (weaker long-range dipolar interaction) and strong two-spin (predominantly nearest neighbor) interactions. Significantly, lower p_c found in other mixtures of the Sm-C phase chiralized with chiral molecules, can be rationalized by noting their larger intrinsic polarization compared to DOBAMBC resulting in larger z (effective coordination number), i.e., $z \propto P$.

In this model, the disappearance of $P_m(x)$ should follow the conductivity, the exponent of which, 2.0, is consistent with our fit shown in Fig. 3(a).

In summary, the first order nature of the C-C^* transition [i.e., discontinuities in q and $P_m(x)$], the quadratic composition dependence of $T_{AC(*)}$, and the topology of the phase diagram suggest that an ACC^* LP can be realized in *mixtures* of liquid crystals.

Financial support from the Petroleum Research Fund (PRF), the gift of ITO plates from Dr. P. Bos (Tektronix Inc.), and numerous discussions with Professor M. Silverberg are gratefully acknowledged.

* Present address: Department of Physics, Nagarjuna University, Nagarjuna Nagar, India.

† Present address: Department of Chemistry, Harvard University, Cambridge, MA 02138.

[1] R. M. Hornreich, M. Luban, and S. Shtrikman, Phys. Rev. Lett. **35**, 1678 (1975); Phys. Lett. **55A**, 269 (1975).

[2] Y. Shapira, in *Multicritical Phenomena*, edited by R. Pynn and A Skjeltorp, NATO ASI Ser. B, Vol. 106 (Plenum, New York, 1983), p. 53.

[3] G. Gompper and M. Schick, Phys. Rev. B **41**, 9148 (1990); M. Teubner and R. Strey, J. Chem. Phys. **87**, 3195 (1987).

[4] P. G. de Gennes, *Physics of Liquid Crystals* (Oxford, New York, 1974), Chap. 5; S. Chandrasekhar, *Liquid Crystals* (Cambridge, New York, 1992).

[5] J. H. Chen and T. Lubensky, Phys. Rev. A **14**, 1202 (1976).

[6] C. R. Safinya, L. J. Martinez-Miranda, M. Kaplan, J. D. Litster, and R. J. Birgeneau, Phys. Rev. Lett. **50**, 56 (1983).

[7] (a) I. Musevic, B. Zeks, R. Blinc, Th. Rasing, and P. Wyder, Phys. Rev. Lett. **48**, 192 (1982); (b) A. Michelson, Phys. Rev. Lett. **39**, 464 (1977); (c) R. Blinc, in *Phase Transitions in Liquid Crystals*, edited by S. Martellucci and A. N. Chester, NATO ASI Series, Vol. 290 (Plenum Press, New York, 1992), Chap. 22; (d) T. Povse, I. Musevic, B. Zeks, and R. Blinc, Liq. Cryst. **14**, 1587 (1993).

[8] R. B. Meyer, L. Liebert, L. Strzelecki, and P. Keller, J. Phys. (Paris), Lett. **36**, L69 (1975).

[9] N. A. Clark and S. T. Lagerwall, Appl. Phys. Lett. **36**, 899 (1980).

[10] G. Spruce and R. D. Pringle, J. Phys. E **21**, 268 (1988); K. Miyasato, S. Abe, H. Takezoe, A. Fukuda, and E. Kuze, Jpn. J. Appl. Phys. **22**, L661 (1983).

[11] C. C. Huang and S. C. Lien, Phys. Rev. A, **31**, 2621 (1985), and references cited therein; S. Dumrongrattana, C. C. Huang, G. Nounesis, S. C. Lien, and J. M. Viner, *ibid.* **34**, 5010 (1986); M. Meichle and C. W. Garland, *ibid.* **27**, 2624 (1983); R. J. Birgeneau, C. W. Garland, A. R. Kortan, J. D. Litster, M. Meichle, B. M. Ocko, C. Rosenblatt, L. J. Yu, and J. Goodby, *ibid.* **27**, 1251 (1983); B. R. Ratna, R. Shashidhar, G. S. Nair, and S. K. Prasad, *ibid.* **37**, 1824 (1988).

[12] T. Carlsson, B. Zeks, C. Filipic, A. Levstik, and R. Blinc, Mol. Cryst. Liq. Cryst., **163**, 11 (1988).

[13] S. B. Rananavare, V. G. K. M. Pisipati, and E. W. Wong, in Proceedings of IS&T/SPIE Symposium, San Jose, February 1994 (to be published).

[14] The C-C^* line will shift towards a higher concentration of DOBAMBC when the bulk pitch length becomes comparable to the cell thickeness. The theory in the strong anchoring limit, as developed in Ref. 7(d), predicts a critical cell thickness, $d_c \propto p$, for the C-C^* transition. However, the C-C^* line in Fig. 1 was determined in thick cells [i.e., d(cell thickness)$> 6p$]. Further studies implying a linear variation of the C-C^* transition line as a function of composition at a fixed reduced temperature in the temperature, thickness, and composition space will be valuable, and they are planned.

[15] S. Redner and E. Stanley, Phys. Rev. B **16**, 4901 (1977); W. Selke, Solid State Commun. **27**, 1417 (1978).

[16] The vertical line shown in Fig. 1 is only schematic; otherwise, the phase diagram suggests four-phase coexistence of FF^*GG^* or C^*CF^*F phases in direct contradiction with the phase rule. However, in our studies, especially near the ACC^* point, equilibration times exceeded 12–24 h. Because of the narrow C^*/C phase extent which is delimited by the first order C-$F(F^*)$ transition, and also due to the well-known drift [11] of the AC^* transition drift at these temperatures, this region of the phase diagram has not yet been extensively examined.

[17] R. B. Stinchcombe, Phase Transitions **7**, 151 (1983).